ACS APPLIED MATERIALS & INTERFACES

www.acsami.org

Research Article

Construction of a Mesoporous Ceria Hollow Sphere/Enzyme Nanoreactor for Enhanced Cascade Catalytic Antibacterial Therapy

Jing Qin, Youyou Feng, Dong Cheng, Biwu Liu, Zheng Wang, Yongxi Zhao, and Jing Wei*

Cite This: https://doi.org/10.1021/acsami.1c10821

Read Online

ACCESS | Metrics & More | Article Recommendations | Supporting Information

ABSTRACT: Nanozyme has been regarded as one of the antibacterial agents to kill bacteria via a Fenton-like reaction in the presence of H_2O_2. However, it still suffers drawbacks such as insufficient catalytic activity in near-neutral conditions and the requirement of high H_2O_2 levels, which would minimize the side effects to healthy tissues. Herein, a mesoporous ceria hollow sphere/enzyme nanoreactor is constructed by loading glucose oxidase in the mesoporous ceria hollow sphere nanozyme. Due to the mesoporous framework, large internal voids, and high specific surface area, the obtained nanoreactor can effectively convert the nontoxic glucose into highly toxic hydroxyl radicals via a cascade catalytic reaction. Moreover, the generated glucose acid can decrease the localized pH value, further boosting the peroxidase-like catalytic performance of mesoporous ceria. The generated hydroxyl radicals could damage severely the cell structure of the bacteria and prevent biofilm formation. Moreover, the *in vivo* experiments demonstrate that the nanoreactor can efficiently eliminate 99.9% of bacteria in the wound tissues and prevent persistent inflammation without damage to normal tissues in mice. This work provides a rational design of a nanoreactor with enhanced catalytic activity, which can covert glucose to hydroxyl radicals and exhibits potential applications in antibacterial therapy.

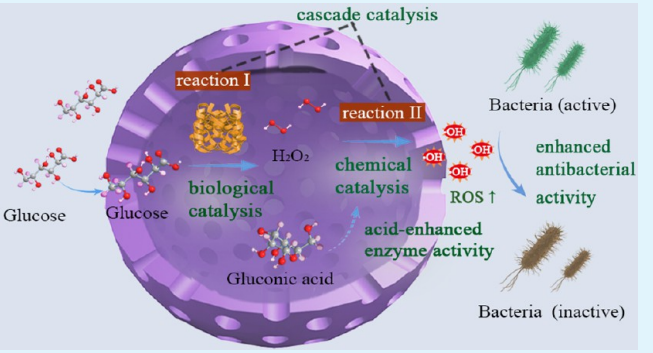

KEYWORDS: *mesoporous material, hollow sphere, ceria, catalysis, antibacterial therapy*

1. INTRODUCTION

Bacterial infection-related diseases have threatened human's health for a long time.[1] The abuse of traditional antibiotic penicillin can result in the generation of bacteria resistance.[2] It is highly desirable to develop a novel antibacterial agent to combat bacterial infections. H_2O_2 is a commonly used antibacterial agent in the application of hygienic and medical treatments. Recently, nanozyme with peroxidase-like activity has been found to effectively convert H_2O_2 to hydroxyl radicals with high toxicity. Compared to H_2O_2, such free radicals can effectively destroy the cell wall of bacteria through an advanced oxidation process.[3−9] The peroxidase-like activity of nanozyme usually relies on the pH value.[10−12] However, a majority of nanozyme exhibits enhanced activity in acidic conditions. The nanozyme shows an unsatisfied catalytic activity in living systems due to near-neutral conditions. Moreover, due to the consumption of free radicals by glutathione *in vivo*, a high H_2O_2 level is usually required to generate enough hydroxyl radicals for antibacterial application.[13−15] However, a high H_2O_2 level not only causes immunogenicity and inflammation but also has high toxicity to normal tissues.[16] Therefore, a catalytic system with high catalytic activity to generate enough hydroxyl radicals is highly required.

Metal oxide hollow spheres (MOHSs) show tunable metal species, nanoporous shells, and large internal voids.[17−20] Due to the nanoporous shell, the materials exhibit a large amount of easily accessible active sites and low diffusion resistance. The large internal voids can act as a small container to load metal nanoparticles, nucleic acids, enzymes, and drugs. Consequently, MOHSs have attracted ever-increasing interests owing to their broad applications in drug/gene delivery, catalysis, and energy conversion and storage.[21−25] CeO_2 nanomaterials show unique features such as good biocompatibility, low cost, and abundant oxygen vacancy defects.[26−32] CeO_2 nanomaterials have been regarded as a versatile artificial enzyme, and include catalase, superoxide dismutase, peroxidase, and haloperoxidase.[33] The fabrication of mesoporous CeO_2 hollow spheres is an attractive strategy to enhance the catalytic performance and endow the materials with new functions.[34] Generally, the mesoporous CeO_2 hollow sphere

Received: June 10, 2021
Accepted: August 10, 2021

Scheme 1. Schematic Illustration of the Construction of a Mesoporous CeO_2 Hollow Sphere/Enzyme Nanoreactor and the Cascade Catalytic Antibacterial Therapy

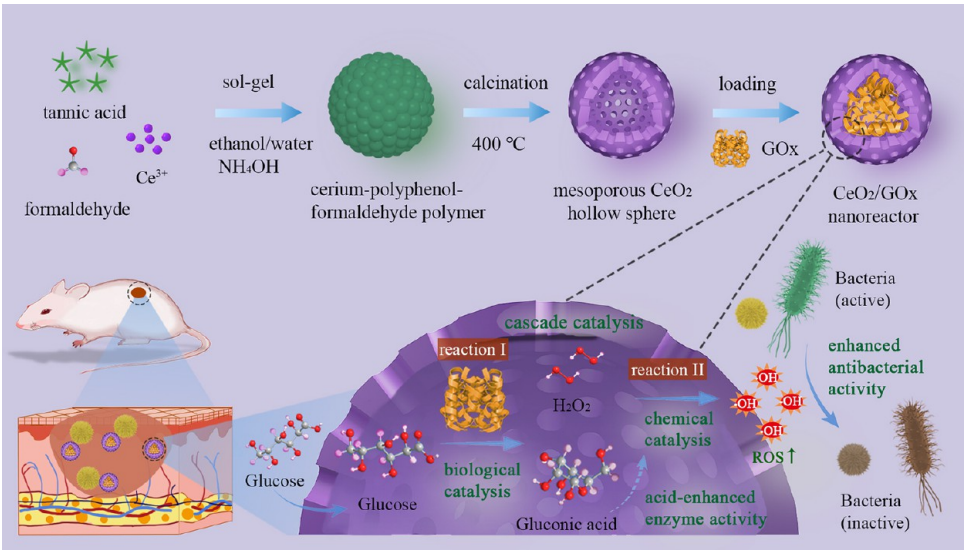

nanozyme exhibits four advantages. First, the hollow spheres show large internal voids. The large voids can accommodate guest nanoparticles or enzymes to further enhance the catalytic performance via a cascade reaction or synergetic effects. Second, when the hollow spheres are used as a container to load the natural enzymes, the inorganic shell can protect the enzyme and improve its stability and reusability. Third, the CeO_2 hollow spheres show nanoporous shells, which can facilitate mass transport and lower the transfer resistance. Comparing with other nanoporous supports, such as metal–organic frameworks (MOFs), CeO_2 hollow spheres show higher acidic stability. The acidic stability is very important when referring to the tumor microenvironment (pH: ~6.0).[35] Lastly, CeO_2 itself shows enzymatic activity including superoxide dismutase, catalase, and peroxidase under different conditions. By combining with other nanoparticles or natural enzymes (e.g., glucose oxidase, GOx), CeO_2 hollow spheres exhibit various functions in biomedical applications. Until now, a variety of supports including hollow mesoporous silica (MSN),[36−38] polymers,[39−41] MOFs,[42−46] and magnetic metal oxide[35,47] have been used to load GOx to construct nanoreactors for cascade catalytic antibacterial or anti-tumor therapy. Compared to these materials, mesoporous CeO_2 hollow spheres show three advantages. First, compared with MSN and polymers only as a carrier, mesoporous CeO_2 hollow spheres can not only be used as a support to load GOx, but also show peroxidase-like catalytic activity. They can build a cascade-catalysis nanoreactor with GOx directly, without using other catalytic components. Second, mesoporous CeO_2 hollow spheres exhibit a stable framework under harsh conditions. Other nanoporous nanoreactors, such as MOFs, are usually not stable in acidic conditions. Third, some metal oxide nanomaterials show enzyme-like activity. They cannot load GOx due to the lack of mesopores and hollow structures. Therefore, mesoporous CeO_2 hollow spheres could be a potential ideal nanoreactor for cascade catalytic antibacterial treatment. To the best of our knowledge, mesoporous CeO_2 hollow spheres, as both a nanoreactor and nanozyme, have been rarely investigated to combat bacteria for wound healing *in vivo*.

Herein, an enzymatic cascade catalytic nanoreactor is constructed by encapsulation of glucose oxidase in the mesoporous ceria hollow spheres (Scheme 1). Cerium–polyphenol–formaldehyde polymer spheres are prepared using Ce^{3+} as a metal source, polyphenol as an organic ligand, formaldehyde as a crosslinker in an alkaline CH_3CH_2OH/H_2O system. After direct thermal decomposition of the polymer spheres, mesoporous ceria hollow spheres are obtained. They show a high specific surface area (30.7 m^2/g) and pore volume (0.36 cm^3/g), a large pore size (5.8 nm), and a uniform diameter (105 nm). After loading of GOx, the CeO_2/GOx nanoreactor is constructed. The glucose can be converted to gluconic acid by GOx. The gluconic acid generated in the nanoreactor could decrease the pH value in the reaction system, which can effectively boost the peroxidase-like catalytic activity of the spherical mesoporous CeO_2 nanozymes. As a result, the H_2O_2 molecules can be effectively converted into hypertoxic hydroxyl radicals. The constructed CeO_2/GOx nanoreactor is further used for antibacterial therapy. The highly toxic hydroxyl radicals can effectively kill bacteria and prevent biofilm formation. Furthermore, the *in vivo* experiments demonstrate that the CeO_2/GOx nanoreactor can avoid bacterial infections and increase the healing rate of wounds of mice.

2. EXPERIMENTAL SECTION

2.1. Preparation of Mesoporous Ceria Hollow Spheres and a CeO_2/GOx Nanoreactor. Mesoporous ceria hollow spheres were synthesized by the self-template process. Typically, PEG (0.1 g) was dissolved in the solution containing water/ethanol (37/8 mL) and ammonia solution (0.35 mL). After stirring for 1 h, 8 mL of tannic acid solution (0.025 g/mL) was added to the above solution. After 5 min, 0.38 mL of formaldehyde solution (37 wt %) was added. After 24 h, 2 mL of $Ce(NO_3)_3$ aqueous solution (35 mg/mL) was added. After 12 h, the solution was subjected to the hydrothermal treatment (100 °C, 12 h). The products were collected and dried. The mesoporous CeO_2 hollow spheres were prepared through direct thermal decomposition of polymers at 400 °C in air. The synthesis of ceria nanoparticles and ceria cubes is shown in Supporting Information. GOx (6 mg) was added to the mesoporous ceria hollow sphere solution (10 mg/mL). After 6 h, the CeO_2/GOx was obtained by centrifugation.

https://doi.org/10.1021/acsami.1c10821
ACS Appl. Mater. Interfaces XXXX, XXX, XXX−XXX

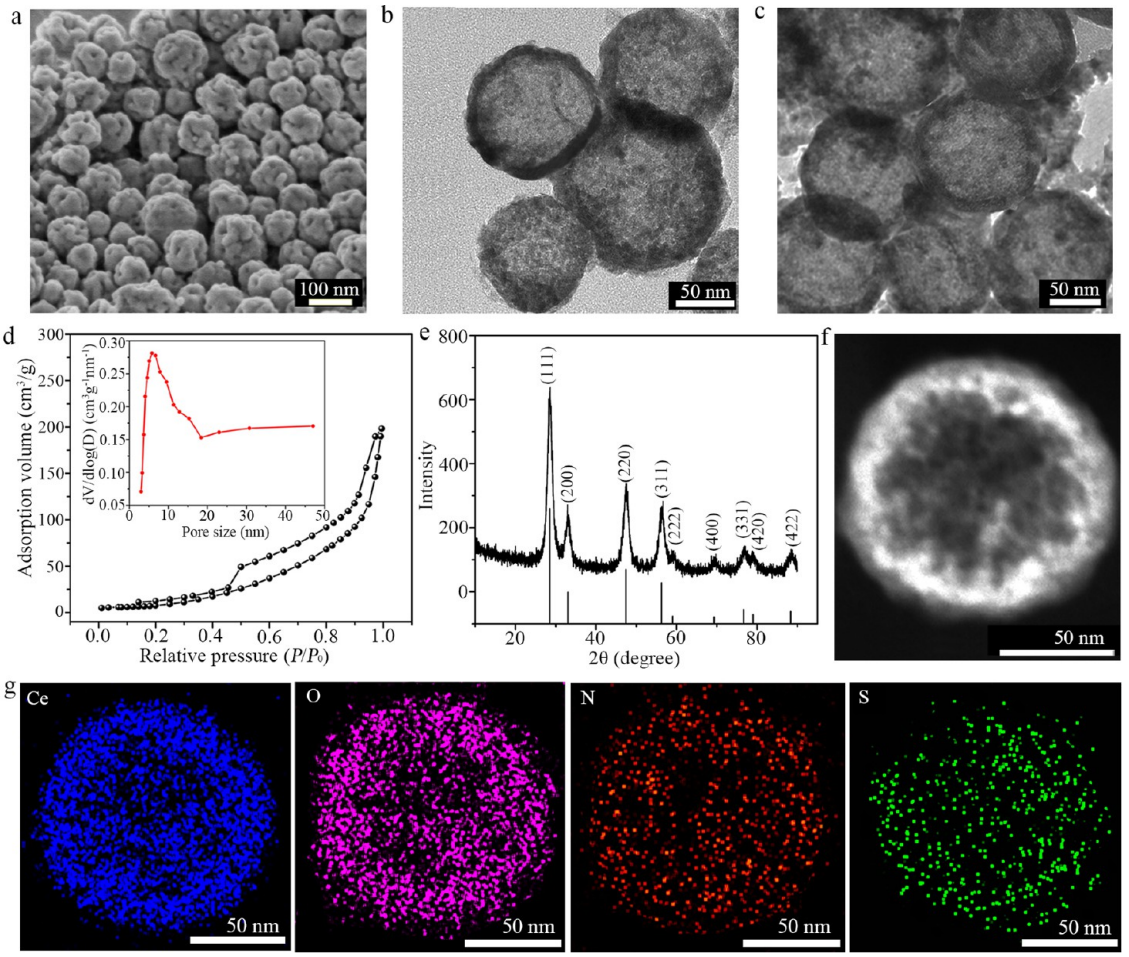

Figure 1. (a) SEM and (b) TEM images of the mesoporous CeO_2 hollow sphere. (c) TEM image of the CeO_2/GOx nanoreactor. (d) N_2 sorption isotherms and pore size distributions (inset) for the mesoporous CeO_2 hollow sphere. (e) XRD patterns of the mesoporous CeO_2 hollow sphere. (f) TEM image and (g) the corresponding element mapping for the CeO_2/GOx nanoreactor.

2.2. Peroxidase-like Activity of Mesoporous CeO_2 Hollow Spheres. Experiments were performed in a 500 μL reaction system (10 mM PBS buffer, pH 4.0), including CeO_2 (10 μg/mL), TMB (0.8 mM), and H_2O_2 (5 mM). The maximum activity of CeO_2/GOx or GOx was regarded as 100%. The residual catalytic activity of CeO_2/GOx or GOx was regarded as the percent of the maximum activity. CeO_2/GOx was incubated at various pH values (3.0−7.0) or temperatures (4−70 °C) for 4 h.

The Michaelis−Menten steady-state catalytic kinetics was explored in the reaction system that contained CeO_2 nanozyme, TMB (0.8 mM), and H_2O_2 at various concentrations (5, 10, 20, 30, 40, and 50 mM). The calculation was according to the previous report.[35]

2.3. Detection of Hydroxyl Radical (·OH). The formation of ·OH was detected using the fluorescent assay. *o*-Phenylenediamine (OPD) and terephthalic acid were used as fluorescent probes. The ·OH can convert the nonfluorescent compounds OPD and terephthalic acid into the high fluorescent product 2,3-diaminophenazine (λ_{em} = 572 nm) and 2-hydroxy terephthalic acid (λ_{em} = 435 nm), respectively.

For OPD, the reaction solution contained (1) OPD, (2) OPD + H_2O_2, (3) OPD + CeO_2, (4) OPD + H_2O_2 + CeO_2, and (5) OPD + glucose + CeO_2/GOx. The experimental conditions were as follows: 0.3 mM OPD, 1 mM H_2O_2, 5 mM glucose, 10 μg/mL CeO_2, or CeO_2/GOx. After reaction for 4 h, a fluorescence spectrophotometer was used to monitor the fluorescence spectra of the product 2,3-diaminophenazine.

For terephthalic acid, the reaction solution contained (1) terephthalic acid, (2) terephthalic acid + H_2O_2, (3) terephthalic acid + CeO_2, (4) terephthalic acid + H_2O_2 + CeO_2, and (5) terephthalic acid + glucose + CeO_2/GOx. The experimental conditions were as follows: 0.5 mM terephthalic acid, 5 mM H_2O_2, 5 mM glucose, 10 μg/mL CeO_2, or CeO_2/GOx. After 12 h, the fluorescence spectra of the product 2-hydroxy terephthalic acid were recorded.

2.4. Bacterial Culture. The monoclonal of *E. coli* and *S. aureus* from the solid Luria−Bertani (LB) medium were transferred and cultured in the liquid LB medium for 12 h (37 °C, 180 rpm). When the logarithmic phase was reached, the bacteria solutions were diluted with PBS to a concentration of 10^7 CFU/mL.

2.5. *In Vitro* Antibacterial Activity. The bacterial solution (0.1 mL, OD: 600 nm at 0.1) received different treatments: (1) PBS, (2) glucose, (3) glucose + CeO_2, (4) CeO_2/GOx, (5) glucose + GOx, and (6) glucose + CeO_2/GOx. The concentrations of CeO_2/GOx and glucose used in the experiment were 100 μg/mL and 15 mM, respectively. After 5 h, the absorbance was recorded. The above-treated groups were reacted for 5 h (37 °C, 180 rpm). Then, the bacterial suspension was diluted 1000 times. The diluted bacterial suspension (100 μL) was spread on a solid medium and cultured for 24 h. The triplicates of each sample were repeated. The experiments including live and dead cell fluorescence assay, biofilm inhibition, characterization of bacteria, antibacterial performance *in vivo*, and biosafety are shown in the Supporting Information.

3. RESULTS AND DISCUSSION

3.1. Synthesis and Characterization of the CeO_2/GOx Nanoreactor. The CeO_2/GOx enzymatic cascade catalytic nanoreactor was constructed via three steps. First, cerium−

https://doi.org/10.1021/acsami.1c10821
ACS Appl. Mater. Interfaces XXXX, XXX, XXX−XXX

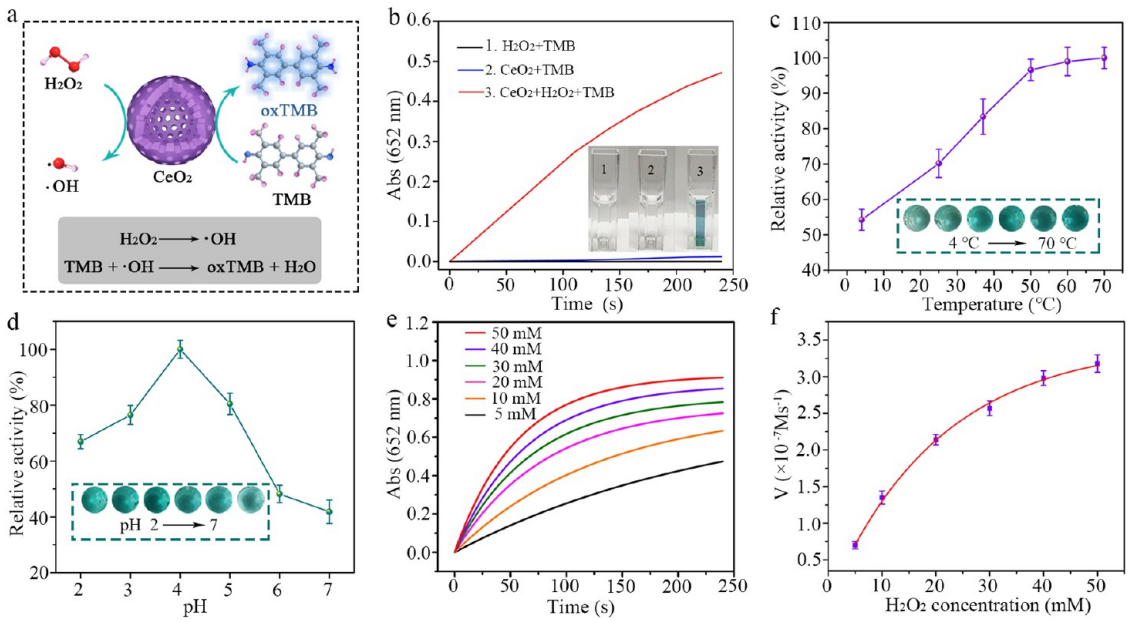

Figure 2. (a) Schematic illustration of the peroxidase-like catalytic process of mesoporous CeO_2 hollow spheres. (b) UV−vis absorbance versus reaction time at 652 nm: (1) H_2O_2 + TMB, (2) CeO_2 + TMB, and (3) CeO_2 + H_2O_2 + TMB. The inset is the corresponding photographs of color evolution in different reaction systems. (c) Peroxidase-like activity of CeO_2 at different temperatures (4, 25, 37, 50, 60, 70 °C). The inset shows the corresponding color change of oxTMB. (d) Peroxidase-like activity of CeO_2 at different pH values at room temperature. The inset shows the corresponding color change of oxTMB. Experiments conditions in (c) and (d): 10 mM PBS buffer, 10 μg/mL CeO_2, 5 mM H_2O_2, and 0.8 mM TMB. (e) Absorbance versus reaction time with different concentrations of H_2O_2: 10 μg/mL CeO_2 nanozyme, 0.8 mM TMB, and 0−50 mM H_2O_2. (f) The corresponding steady-state kinetic assays of CeO_2 for H_2O_2.

polyphenol−formaldehyde polymer spheres were prepared using polyphenol as an organic ligand, Ce^{3+} as a metal source, and formaldehyde as a crosslinker.[48,49] Second, the cerium-based polymers were calcined in air at 400 °C to obtain mesoporous ceria hollow spheres. During the calcination process, the decomposition of the polymer framework led to severe shrinkage. CeO_2 materials with a hollow structure and mesoporous framework were obtained. Third, GOx was encapsulated into the mesoporous ceria hollow spheres owing to the mesoporous framework and large internal voids. Consequently, the CeO_2/GOx nanoreactor was obtained.

The scanning electron microscopic (SEM) and transmission electron microscopic (TEM) images of cerium−polyphenol−formaldehyde polymers showed a solid with a spherical shape (~145 nm) (Figure S1a,b). The metal content in the coordination polymers was 11.6 wt % according to the thermogravimetry (TG) results (Figure S1c). After calcination at 400 °C, the obtained CeO_2 exhibited reserved morphology (~105 nm) (Figure 1a). A large number of nanopores were observed on the surface of the CeO_2 sphere. The TEM image of CeO_2 further revealed the formation of a hollow sphere (Figure 1b). Such hollow spheres were produced due to the severe shrinkage of cerium−polyphenol−formaldehyde polymer spheres.[24] During the calcination process, the solid−air interface of the coordination polymer degrades faster than the interior. Moreover, there is an outward flow of gas (such as CO_2) during the decomposition of the coordination polymer. The cerium species in the sphere may migrate along with the outward gas flow, forming a metal oxide dense layer. The metal oxide dense layer will convert to a mesoporous framework due to the crystal growth of the metal oxide.[25] The N_2 sorption isotherms revealed the mesoporous framework (Figure 1d). The pore size, total pore volume, and specific surface area were 5.8 nm, 0.36 cm^3/g, and 30.7 m^2/g, respectively. The X-ray diffraction (XRD) patterns for mesoporous CeO_2 hollow spheres revealed nine diffraction peaks (Figures 1e and S1d), which were ascribed to the cubic fluorite CeO_2 (JCPDS-no. 34-0394).[50] X-ray photoelectron spectroscopy (XPS) analysis of the mesoporous CeO_2 hollow sphere revealed the presence of Ce species (Figure S2). The peaks u, v, u'', v'', u''', and v''' at 901.1, 882.6, 907.4, 888.7, 916.8, and 898.5 eV, respectively, were ascribed to Ce^{4+}.[51,52] The peaks u' and v' with binding energies of 902.9 and 885.4 eV were ascribed to Ce^{3+}. The contents of Ce^{3+} and Ce^{4+} were 15.19 and 84.81%, respectively. The enzyme-like activity of ceria was related to the Ce^{3+}/Ce^{4+} ratio.[53−58] In the mesoporous CeO_2 hollow sphere, the ratio of Ce^{3+}/Ce^{4+} was around 1.0:5.6, determined by the XPS results.

Due to the mesoporous framework and large internal voids for CeO_2, glucose oxidase (GOx) was further loaded in the mesoporous CeO_2 hollow spheres to construct the CeO_2/GOx nanoreactor. The TEM image of the CeO_2/GOx nanoreactor showed a spherical hollow structure, which was like the mesoporous CeO_2 hollow sphere (Figure 1c). In contrast, the elemental mapping of the CeO_2/GOx nanoreactor showed the presence of N and S elements (Figure 1f,g). The elemental linear scanning for N and S further indicated that GOx was encapsulated in the mesoporous CeO_2 hollow spheres (Figure S3a−c). By comparison, the element mapping of the mesoporous CeO_2 hollow spheres without loading of GOx showed negligible N and S elements in the framework (Figure S3d−f). The element mapping results indicated successful encapsulation of GOx in the mesoporous CeO_2 hollow sphere. The loading amount of GOx was around 6.67 wt %, calculated using the BCA Protein Assay Kit (Figure S4). The ζ-potential decreased from +20.3 to −11.5 mV after loading of GOx (Figure S5a), indicating that a part of GOx molecules may be

https://doi.org/10.1021/acsami.1c10821
ACS Appl. Mater. Interfaces XXXX, XXX, XXX−XXX

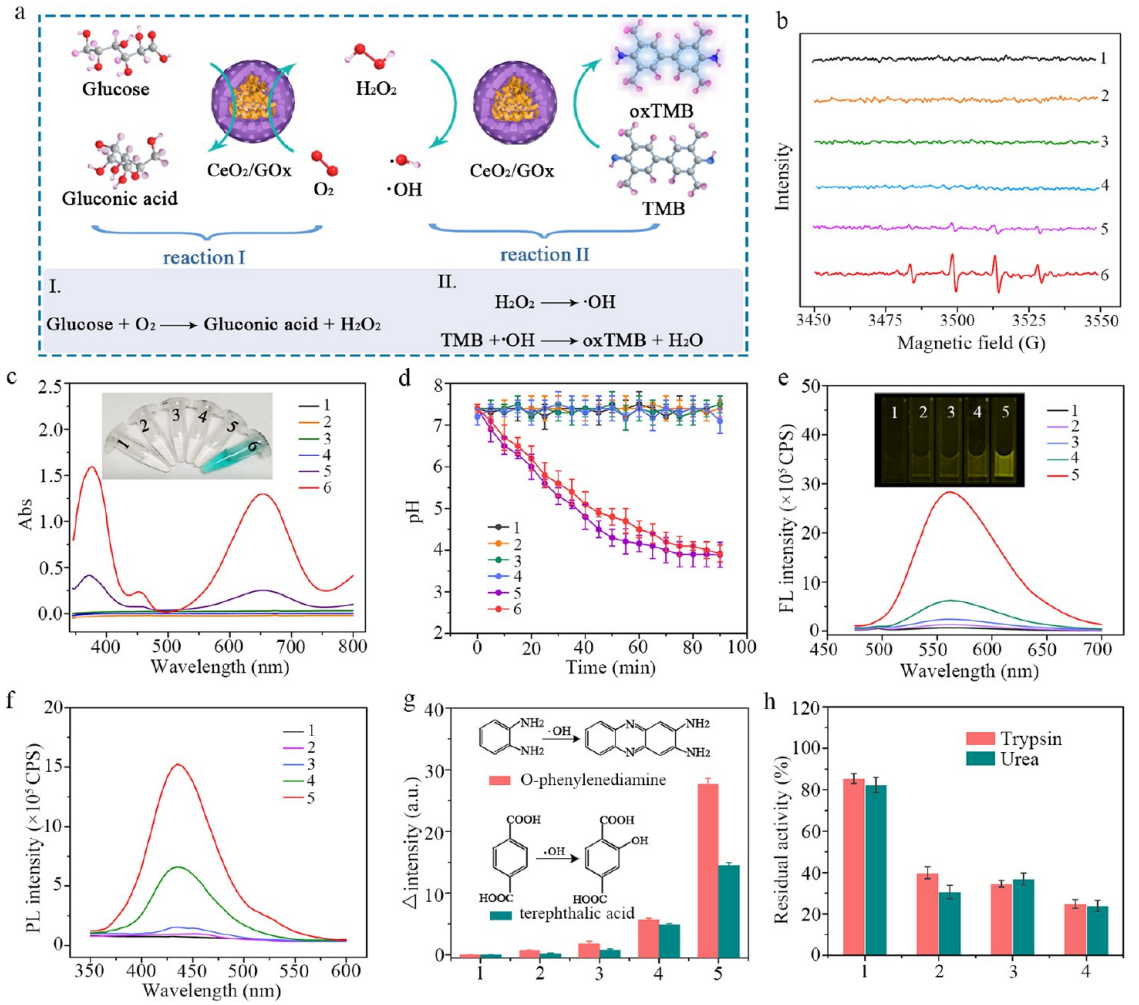

Figure 3. (a) Schematic illustration of the cascade catalytic reaction in the CeO_2/GOx nanoreactor. (b) EPR spectroscopy of different groups using DMPO (8.8 mM) as a trapping agent. (c) UV−vis absorbance spectra in different systems. Insets in (c) are the corresponding photographs. (d) The pH value versus reaction time under different conditions. Experiments (1−6) in (b−d) were performed in PBS buffer (0.5 mM): PBS, glucose, glucose + CeO_2, CeO_2/GOx, glucose + GOx, and glucose + CeO_2/GOx. Experimental conditions: 5 mM glucose, 10 μg/mL CeO_2 or CeO_2/GOx, and 0.5 μg/mL GOx. (e) Typical fluorescence spectra of *o*-phenylenediamine (OPD) catalyzed by different groups: (1) OPD, (2) OPD + H_2O_2, (3) OPD + CeO_2, (4) OPD + H_2O_2 + CeO_2, and (5) OPD + glucose + CeO_2/GOx. Inset in (e) shows the fluorescence image of *o*-phenylenediamine (OPD) oxidation catalyzed by different groups. Experimental conditions: 0.3 mM OPD, 1 mM H_2O_2, 5 mM glucose, and 10 μg/mL CeO_2 or CeO_2/GOx. (f) Typical fluorescence spectra of terephthalic acid oxidation catalyzed by different groups: (1) terephthalic acid, (2) terephthalic acid + H_2O_2, (3) terephthalic acid + CeO_2, (4) terephthalic acid + H_2O_2 + CeO_2, and (5) terephthalic acid + glucose + CeO_2/GOx. (g) The corresponding fluorescence intensity of different groups in (e) and (f). The error bars reflect mean ± standard deviation (n = 3). (h) Residual catalytic activity of GOx in different groups: (1) CeO_2/GOx nanoreactor, (2) CeO_2 cube@GOx, (3) CeO_2 nanoparticles@GOx, and (4) free GOx in the presence of trypsin (20 μg/mL) or urea (2 M) for 1 h.

adsorbed on the material surface. The hydrodynamic size increased from 105 to 134 nm after loading of GOx (Figure S5b). The sodium dodecyl sulfate-polyacrylamide gel electrophoresis results revealed that the bands of CeO_2/GOx were consistent with that of pure GOx (80 kD) (Figure S6). These results demonstrated the successful construction of the CeO_2/GOx nanoreactor.

3.2. Catalytic Activity of the CeO_2/GOx Nanoreactor. The peroxidase-like activity of mesoporous CeO_2 hollow spheres was investigated via the catalytic oxidation of 3,3′,5,5′-tetramethylbenzidine (TMB) (Figure 2a). Mesoporous CeO_2 hollow spheres could catalyze the oxidation of TMB using H_2O_2 as an oxidant to produce oxTMB, with a characteristic absorption peak at 652 nm (Figure 2b). In the absence of CeO_2 or H_2O_2, negligible color and absorbance changes were observed. These results confirmed that mesoporous CeO_2 hollow spheres showed peroxidase-like activity. The effects of temperature and pH on the catalytic activity of mesoporous CeO_2 hollow spheres were further investigated. The absorbance increased when the temperature increased (Figure 2c). The peroxidase-like activity of the mesoporous CeO_2 hollow sphere reached a maximum when the pH value reached 4.0 (Figure 2d). These results revealed that the CeO_2 nanozyme showed tunable catalytic performance at various conditions (temperature, pH value). Especially, the catalytic activity of mesoporous CeO_2 hollow spheres could be significantly increased when the pH value was decreased from 7 to 4.

To further investigate the catalytic activity of the mesoporous CeO_2 hollow sphere nanozyme, the Michaelis−Menten steady-state catalytic kinetics was determined. The catalytic activity of the mesoporous CeO_2 hollow sphere

https://doi.org/10.1021/acsami.1c10821
ACS Appl. Mater. Interfaces XXXX, XXX, XXX−XXX

nanozyme increased when the concentration of H_2O_2 increased (Figure 2e). For each concentration of H_2O_2, the initial reaction velocities (v_0) could be converted to the initial velocities of the absorbance change of oxTMB using the Beer−Lambert law.[35] The v_0 values versus the concentration of H_2O_2 are plotted (Figure 2f). According to the Michaelis−Menten equation and the linear double-reciprocal plots (Figure S7), the Michaelis−Menten constant (K_M) and maximum velocity (V_{max}) for the mesoporous CeO_2 hollow sphere nanozyme toward H_2O_2 were 28.24 mM and 5.07×10^{-7} M/s, respectively. The K_M and V_{max} for the mesoporous CeO_2 hollow sphere nanozyme toward TMB were 0.285 mM and 7.9×10^{-9} M/s, respectively. The catalytic activity for the mesoporous CeO_2 hollow sphere was among the best of other reported state-of-the-art CeO_2 enzymes (Table S1). The catalytic activity for the mesoporous CeO_2 hollow sphere nanozyme was also comparable to the natural horseradish peroxidase.

The mesoporous CeO_2 hollow spheres showed enhanced peroxidase-like activity when the pH value was changed from 7 to 4. To further improve the catalytic performance, the localized pH value in the nanoreactor should be decreased. Therefore, glucose was used as a substrate due to its nontoxicity compared with H_2O_2. More importantly, glucose can be converted to gluconic acid using GOx as a catalyst. The generated gluconic acid could decrease the localized pH value owing to its acidic property. The acidic condition further boosted the peroxidase-like activity of the mesoporous CeO_2 hollow spheres. The production of gluconic acid was verified with a pH meter and methyl red. The pH values decreased from 7.4 to 4.1 within 90 min when glucose and GOx coexisted (Figure S8a). The color change of the methyl red solution further proved the decrease of the pH value (Figure S8b).

After evaluating the catalytic activity of the mesoporous CeO_2 hollow spheres and GOx, respectively, the cascade catalytic performance of the CeO_2/GOx nanoreactor was further studied. Glucose molecules can be converted to H_2O_2 and gluconic acid in the presence of oxygen (Figure 3a). The generated gluconic acid can decrease the localized pH value in the nanoreactor. The produced H_2O_2 was further catalyzed by mesoporous CeO_2 hollow spheres to generate ·OH under acidic conditions. The hydroxyl radical was determined with electron paramagnetic resonance (EPR) spectra. The generated hydroxyl radical could be captured by 5,5-dimethyl-1-pyrroline *N*-oxide (DMPO) to form DMPO/·OH adducts. The strong EPR spectrum with 1:2:2:1 line, indicated the generation of ·OH in group 6 (Figure 3b). By contrast, there was a negligible EPR signal of DMPO/·OH in groups 1−5. Similarly, the cascade catalytic reaction for the CeO_2/GOx nanoreactor was investigated using TMB as an indicator. The solution showed a characteristic absorption peak at 652 nm for the CeO_2/GOx nanoreactor in the presence of glucose (Figure 3c). There was negligible absorbance in the control experiments. Meanwhile, the pH value for the reaction solution with different treatments was measured. The pH value of the reaction solution remained constant at around 7.4 in experiments 1−4. By contrast, the pH value changed from 7.4 to 4.1 in experiments 5−6 (Figures 3d and S9). The decrease of the pH value indicated the production of glucose acid.

To verify the enhanced catalytic activity, the capability of hydroxyl radicals produced by H_2O_2 + mesoporous CeO_2 hollow spheres and glucose + CeO_2/GOx nanoreactor was investigated. Hydroxyl radicals can convert nonfluorescent compounds (i.e., *o*-phenylenediamine and terephthalic acid) to a highly fluorescent product (i.e., 2,3-diaminophenazine and 2-hydroxy terephthalic acid). The fluorescence intensity for glucose + CeO_2/GOx nanoreactor was higher than that of H_2O_2 + mesoporous CeO_2 hollow spheres and control experiments (Figure 3e−g). These results confirmed that the glucose + CeO_2/GOx nanoreactor could produce more hydroxyl radicals than those of the H_2O_2 + mesoporous CeO_2 hollow spheres. When glucose and CeO_2/GOx nanoreactor coexisted, the produced gluconic acid could decrease the localized pH value and enhance the peroxidase-like activity of mesoporous CeO_2 hollow spheres, thus generating more number of ·OH radicals. Similarly, mesoporous CeO_2 hollow spheres exhibited weak peroxidase-like activity in near-neutral conditions in the presence of H_2O_2 and mesoporous CeO_2 hollow spheres.

CeO_2 nanomaterials also exhibit catalase-like activities, which can decompose H_2O_2 into O_2. The catalase-like activity of the mesoporous CeO_2 hollow sphere at different pH values was investigated (Figure S10). The amount of oxygen generated was the highest at pH 7. Only a very small amount of oxygen was produced at pH 4. The cascade catalysis of the CeO_2/GOx nanoreactor could produce a large amount of gluconic acid, resulting in acidic conditions. The catalase-like activity can be effectively inhibited, which is beneficial to produce highly toxic hydroxyl radicals.

The relationship between the GOx content and the catalytic properties of the CeO_2/GOx nanoreactors was also investigated (Figure S11). When the loading amount of GOx increased from 1.02 to 9.87%, the relative catalytic activity of the nanoreactor also increased. This was because more glucose molecules were converted into H_2O_2 by GOx. Further increase of the GOx amount may block the mesopores and limit mass transport.

The stability of GOx after being encapsulated in the mesoporous CeO_2 hollow spheres was also investigated. For comparison, CeO_2 cubes and CeO_2 nanoparticles were prepared (Figure S12). GOx molecules were also loaded on the CeO_2 cubes and nanoparticles. The enzyme retention activities of the CeO_2/GOx nanoreactor, CeO_2 cubes@GOx, CeO_2 nanoparticles@GOx, and free GOx were investigated after denaturation. The bioactivity of trypsin-treated CeO_2/GOx was 85.4% of that observed prior to trypsin treatment, which was significantly higher than those of CeO_2 cubes@GOx (39.9%), CeO_2 nanoparticles@GOx (34.6%), and free GOx (24.8%) (Figure 3h). The mesoporous CeO_2 hollow sphere could protect the GOx from hydrolysis by trypsin. Urea molecules can disrupt the interior hydrogen bonds of proteins and lead to protein unfolding.[59] The retained bioactivity of urea-treated CeO_2/GOx was 82.5% that prior to urea treatment. By comparison, the bioactivities of urea-treated CeO_2 cubes@GOx, CeO_2 nanoparticles@GOx, and free GOx dramatically decreased to 30.6, 36.9, and 23.9% of that without treatment by urea (Figure 3h). Due to the large internal voids, the GOx molecules can be encapsulated in hollow spheres. The mesoporous CeO_2 hollow sphere could act as a protective layer to enhance the stability of GOx.

3.3. Antibacterial and Biofilm Inhibition Performance *In Vitro*.

Encouraged by the enhanced catalytic activity of the CeO_2/GOx nanoreactor in the presence of glucose, the antibacterial performance against both Gram-positive *Staphylococcus aureus* and Gram-negative *Escherichia coli* was studied.

https://doi.org/10.1021/acsami.1c10821
ACS Appl. Mater. Interfaces XXXX, XXX, XXX−XXX

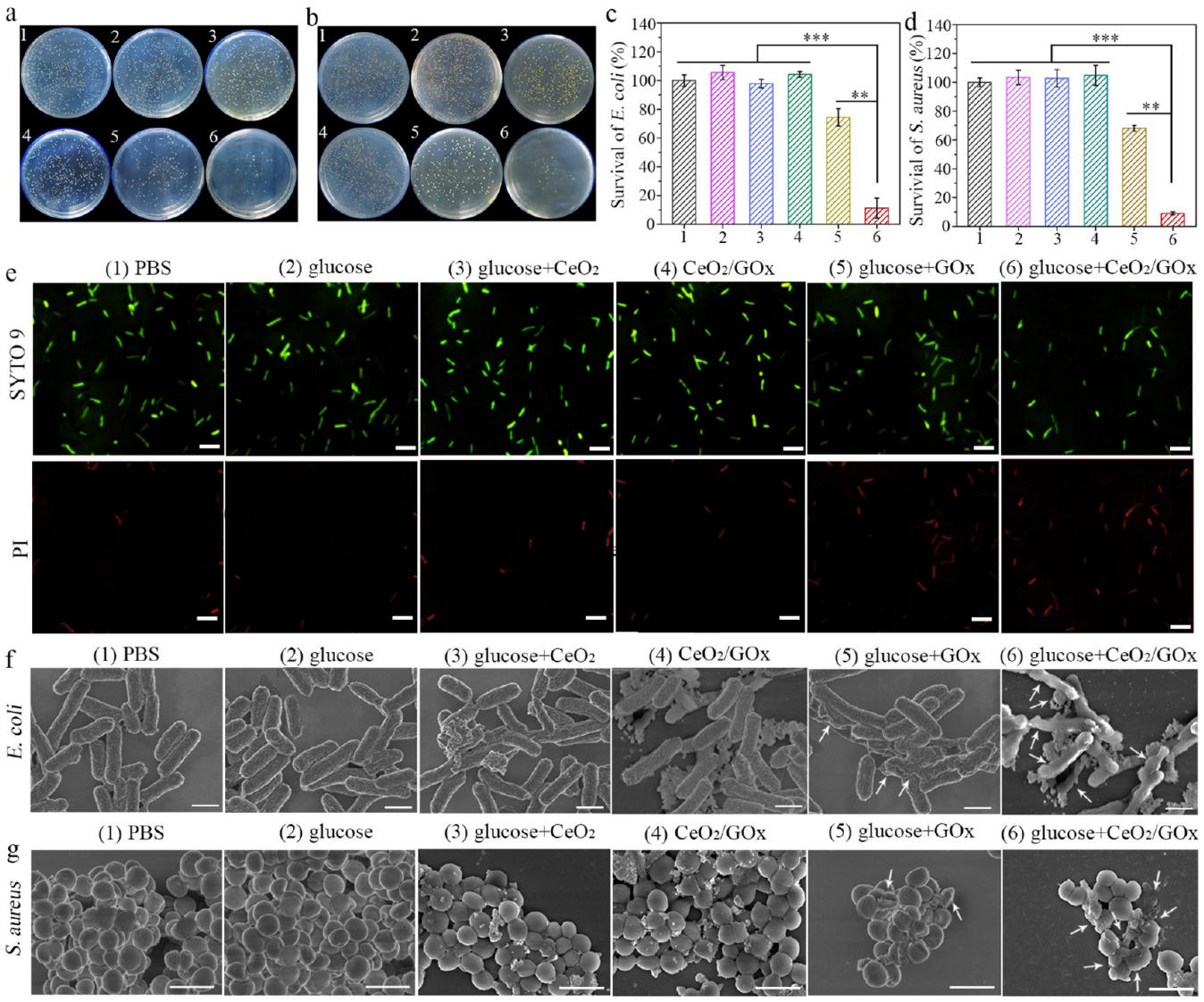

Figure 4. Photographs of bacterial colonies formed by (a) *E. coli* and (b) *S. aureus*. The relative bacterial survival of (c) *E. coli* and (d) *S. aureus*. (e) Fluorescence images for the live/dead bacterial staining assay of *E. coli*. Scale bar: 5 μm. Typical SEM images of (f) *E. coli* and (g) *S. aureus* after different treatments. Scale bar: 1 μm. The samples were prepared by treating with (1) PBS, (2) glucose, (3) glucose + CeO_2, (4) CeO_2/GOx, (5) glucose + GOx, and (6) glucose + CeO_2/GOx. Experimental conditions (a–d): 15 mM glucose, 100 μg/mL CeO_2 or CeO_2/GOx, and 5 μg/mL GOx. Experimental conditions (e–g): 50 mM glucose, 500 μg/mL CeO_2 or CeO_2/GOx, and 25 μg/mL GOx. The error bars reflect mean ± standard deviation (n = 3).

The effect of the concentration of glucose on the antibacterial performance using CeO_2/GOx nanoreactors was investigated. When the concentration of glucose increased, the antibacterial efficiency of CeO_2/GOx nanoreactors was also enhanced (Figure S13). When the concentration was 15 mM, less than 10% survival rate was observed for bacteria, indicating the high antibacterial ability of the CeO_2/GOx nanoreactors. Subsequently, the antibacterial properties of the CeO_2/GOx nanoreactors were evaluated by treating the bacteria with different groups: (1) PBS, (2) glucose, (3) glucose + CeO_2, (4) CeO_2/GOx, (5) glucose + GOx, and (6) glucose + CeO_2/GOx. The number of bacterial colonies in groups, (2) glucose, (3) glucose + CeO_2, and (4) CeO_2/GOx, was not obviously changed compared to the group (1) with PBS treatment (Figure 4a–d). Such results indicated that glucose, glucose + CeO_2, and the nanoreactor alone exhibited negligible antibacterial capability. In group (5), both glucose (15 mM) and GOx (5 μg/mL) were used. The bacterial viabilities were 74.8 and 70.6% for *E. coli* and *S. aureus*, respectively (Figure 4c,d). This was due to the generation of H_2O_2, which could partially kill the bacteria. The effect of GOx concentration on the antibacterial activity was investigated in group (5). After being treated with glucose + GOx (6.67 and 8 μg/mL), the viabilities of bacteria were 77.5 and 73.2% for *E. coli*, which was close to the viability of bacteria treated with glucose + GOx (5 μg/mL) (Figure S14). Similar results were also found in *S. aureus*. These results indicated the limited antibacterial efficiency in group (5) due to the weak antibacterial activity for H_2O_2. In group (6), glucose (15 mM) and CeO_2/GOx (100 μg/mL) were used. The bacterial colonies were less than 10%. The enhanced antibacterial performance was ascribed to the highly toxic ·OH produced in group (6). Additionally, it was found that the pH value of the bacterial solution decreased from 7.4 to 4.4 (Figure S15a,b). The peroxidase-like activity of

https://doi.org/10.1021/acsami.1c10821
ACS Appl. Mater. Interfaces XXXX, XXX, XXX–XXX

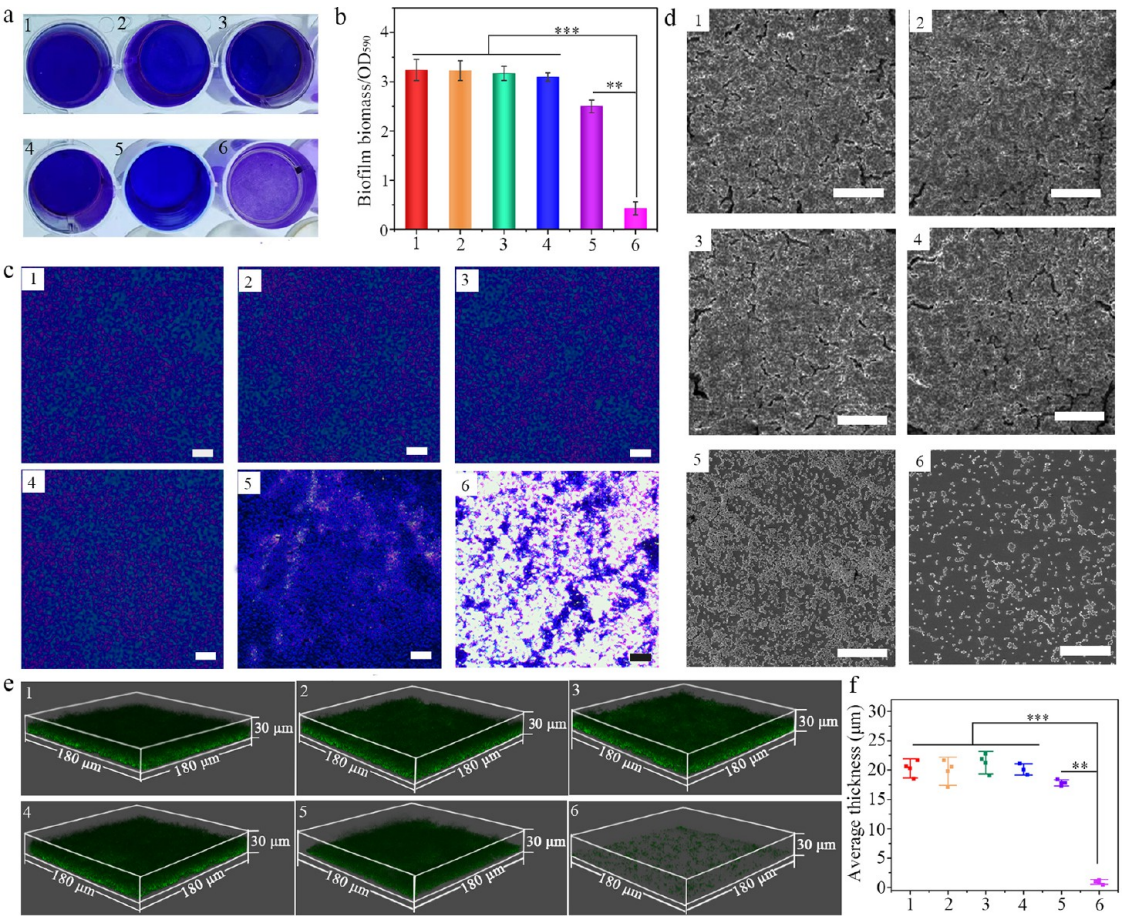

Figure 5. (a) Photographs of crystal-violet-stained biofilm. (b) Biofilm biomass after various treatments. (c) The corresponding microscopy images of crystal-violet-stained biofilm. Scale bar: 20 μm. (d) SEM images of biofilms. Scale bar: 200 μm. (e) 3D CLSM and (f) average thickness of biofilms. The error bars reflect mean ± standard deviation (n = 3). Statistic results: *p < 0.05; **p < 0.01; and ***p < 0.001. Experiments (1−6): (1) PBS, (2) glucose, (3) glucose + CeO_2, (4) CeO_2/GOx, (5) glucose + GOx, and (6) glucose + CeO_2/GOx. Experimental conditions: 15 mM glucose, 100 μg/mL CeO_2 or CeO_2/GOx, and 5 μg/mL GOx.

the mesoporous CeO_2 hollow sphere was activated in the acidic condition.

The antibacterial performance of the mesoporous CeO_2 hollow spheres using H_2O_2 as an oxidant agent was also investigated. When the same concentration of H_2O_2 and glucose was used in the experiment, the group (glucose + CeO_2/GOx) showed higher antibacterial performance than the group (H_2O_2 + CeO_2). The antibacterial efficiencies of the group treated with glucose + CeO_2/GOx (10 mM glucose) reached 80.1 and 83.3% for *E. coli* and *S. aureus* (Figure S16). By comparison, the antibacterial efficiencies for H_2O_2 + CeO_2 group (10 mM H_2O_2) were 38.2 and 43.9% for *E. coli* and *S. aureus,* respectively (Figure S16). The peroxidase-like activity of the mesoporous CeO_2 hollow sphere relied on the pH value. In the group (glucose + CeO_2/GOx), the decrease of the pH value could boost the catalytic activity and the antibacterial effect of the nanoreactor. Moreover, the continuous production of H_2O_2 from glucose and oxygen could avoid the direct introduction of H_2O_2 at high concentrations. As a result, this process could minimize the harmful side effects. Consequently, the designed CeO_2/GOx nanoreactor was a benign antibacterial system.

To further evaluate the antibacterial performance of the CeO_2/GOx nanoreactor, live/dead assays were carried out. *E. coli* cells received different treatments, which were divided into six groups: (1) PBS, (2) glucose, (3) glucose + CeO_2, (4) CeO_2/GOx, (5) glucose + GOx, and (6) glucose + CeO_2/GOx. Most of the *E. coli* cells were alive in groups (1−4) (Figure 4e). In group 5, there are very few red fluorescent cells, indicating the limited antibacterial efficiency. By comparison, the number of dead cells dramatically increased in group 6. This revealed that highly toxic hydroxyl radicals were generated in group 6. Similar inhibition effects were also observed for *S. aureus* via live/dead assays (Figure S17). These results further verified the high antibacterial performance of the CeO_2/GOx nanoreactor in the presence of glucose.

The morphological changes in the bacteria with different treatments were investigated. The SEM image of *E. coli* cells treated with PBS (group one) showed a typical rod shape with clear borders and membrane integrity (Figure 4f). In groups 2−4, there were very few disruptions on the surface of the cell. This indicated a negligible antibacterial effect against *E. coli*. By contrast, the bacterial surface became partially wrinkled in group 5, indicating that the generated H_2O_2 had weak antibacterial activity. It should be noted that in group 6, there was cell wall fragmentation and irregularly shaped holes on the surface of the cell. This indicated severe damage to bacterial membranes. Similar results were also observed for *S. aureus* (Figure 4g). These results indicated that the cell membrane of bacteria was oxidatively damaged by the toxic

https://doi.org/10.1021/acsami.1c10821
ACS Appl. Mater. Interfaces XXXX, XXX, XXX−XXX

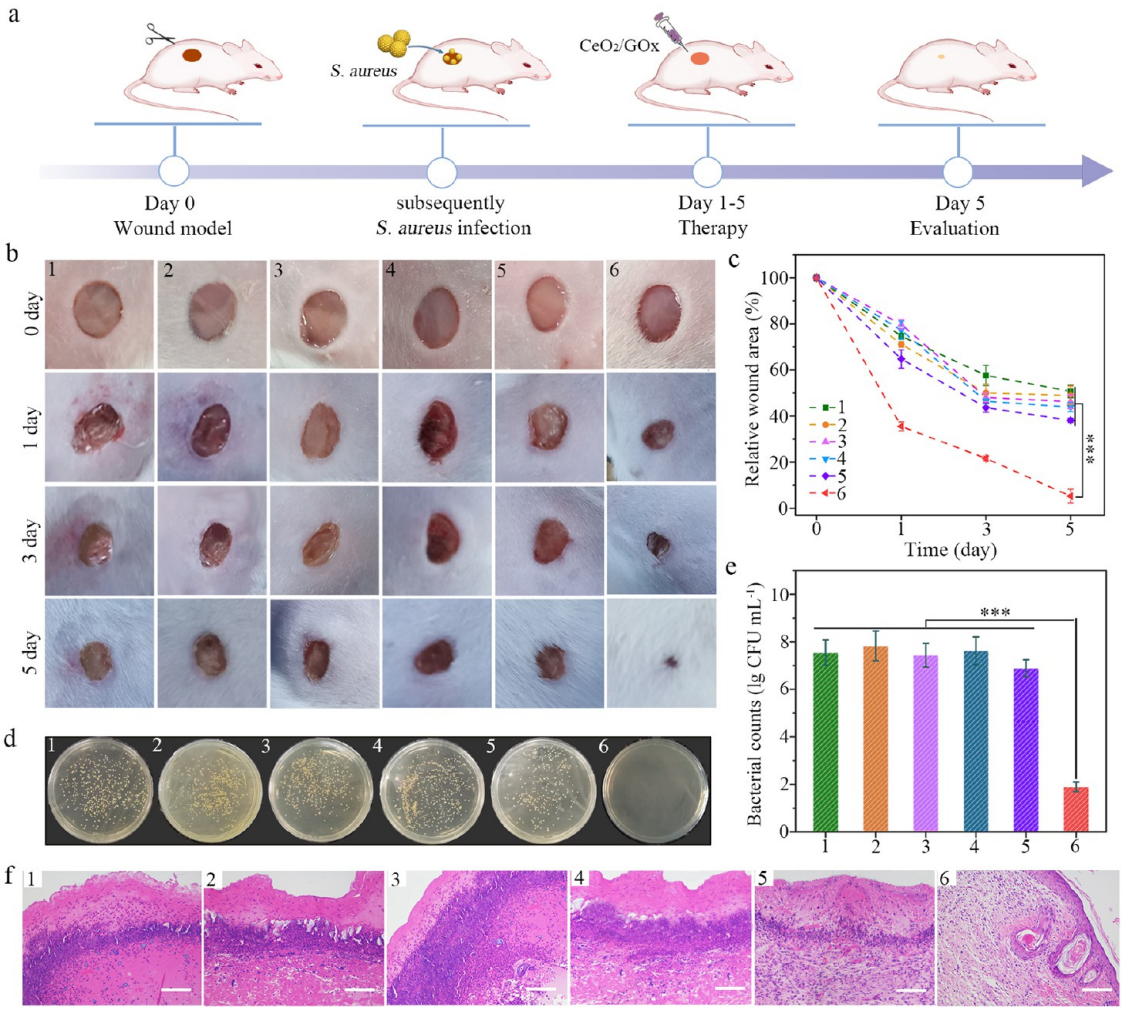

Figure 6. (a) Schematic illustration of the wound-healing experiment. (b) Photographs for wounds of mice infected by *S. aureus* received different treatments. (c) Relative wound area of mice. The error bars reflect mean ± standard deviation (n = 5). (d) Photographs of bacterial colonies formed by bacteria obtained from wound tissues. (e) The number of bacteria in wound tissues. The error bars reflect mean ± standard deviation (n = 5, ***p < 0.001). (f) Histological studies with H&E staining of wounds after different treatments: PBS, glucose, glucose + CeO_2, CeO_2/GOx, glucose + GOx, and glucose + CeO_2/GOx. Experimental conditions: 15 mM glucose, 100 μg/mL CeO_2 or CeO_2/GOx, and 5 μg/mL GOx. Scale bar: 100 μm.

hydroxyl radicals generated from cascade catalysis in the CeO_2/GOx nanoreactor. The integrity of the bacterial cell membrane system was destroyed. The bacteria were severely fragmented and the bacterial contents flow out, leading to bacterial death.[60−63]

Encouraged by the above results, the CeO_2/GOx nanoreactor in the presence of glucose was further used to inhibit biofilm formation. Biofilms contain exopolysaccharide barriers. The inhibition of biofilm formation is usually difficult using antibacterial agents. *S. aureus* was selected as a model to investigate the inhibition efficacy of the CeO_2/GOx nanoreactor against biofilms. *S. aureus* and the tryptone soy broth medium containing different agents, (1) PBS, (2) glucose, (3) glucose + CeO_2, (4) CeO_2/GOx, (5) glucose + GOx, and (6) glucose + CeO_2/GOx, were co-incubated. The concentrations of CeO_2/GOx and glucose were 100 μg/mL and 15 mM, respectively. The inhibition efficacy of the CeO_2/GOx nanoreactor against biofilms was evaluated. The color of the biofilm with different treatments was different (Figure 5a). The color in groups (1−4) was blue, that in group (5) was light blue, and that in group (6) was purple. The enhanced biofilm inhibition effect for the CeO_2/GOx nanoreactor in the presence of glucose was due to the generated hydroxyl radicals with high toxicity. Furthermore, the biomass of the biofilms was measured using crystal violet-based colorimetric assay. The biomass of the biofilm in groups (2−4) was similar to that of group (1), indicating that glucose, glucose + CeO_2, and the CeO_2/GOx nanoreactor alone would not effectively inhibit the formation of the biofilm. The inhibition rate in group (5), glucose + GOx, was 20.7% (Figures 5b and S18). The inhibition rate in group (6) was as high as 90.2%. The corresponding microscopy images of different biofilms also showed the efficient biofilm inhibition effects for the CeO_2/GOx nanoreactor plus glucose (Figure 5c).

The biofilm thickness was measured using a confocal scanning microscope (CLSM). The thickness of groups (1−4) was similar, with an average thickness of around 20.2 μm (Figure 5e,f). The thickness of biofilm in group (5) was 15.7 μm. In group (6), a complete and thick biofilm was not observed. Only scattered colonies of bacteria were seen, suggesting a significant inhibitory effect. Simultaneously, SEM results also suggested the structural changes with various

https://doi.org/10.1021/acsami.1c10821
ACS Appl. Mater. Interfaces XXXX, XXX, XXX−XXX

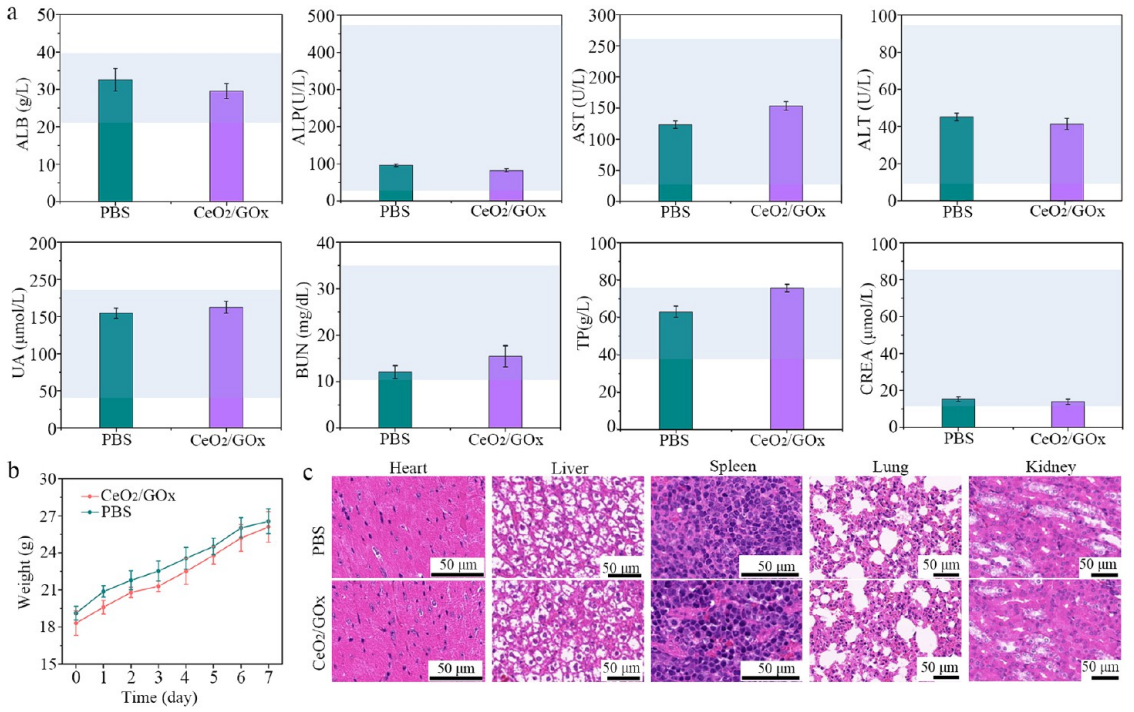

Figure 7. (a) Blood biochemistry indexes of mice treated with PBS or CeO_2/GOx. (b) The body weights of mice versus time. (c) Histological studies of major organs after treatment with PBS or CeO_2/GOx. The error bars reflect mean ± standard deviation (n = 3).

treatments. Almost all of the bacteria in groups (1−4) were aggregated and embedded in exopolysaccharides (EPS). The biofilm was only slightly cleaved in group (5) due to the limited biofilm inhibition efficiency. In contrast, the bacterial biofilm in group (6) was significantly destroyed (Figure 5d), indicating that the CeO_2/GOx nanoreactor could be used to inhibit biofilm formation in the presence of glucose. The effective destruction and elimination of biofilms were due to hydroxyl radicals, which could effectively decompose the bacterial nucleic acids, proteins, and polysaccharide components in the EPS matrix.[64] Therefore, the CeO_2/GOx nanoreactor can effectively cleave the existing biofilms and restrain the generation of new biofilms.

3.4. Antibacterial Performance *In Vivo*. To investigate the antibacterial performance of the CeO_2/GOx nanoreactor *in vivo*, a bacteria-infected mice model was built by the deposition of *S. aureus* on the wound of the back for Kunming mice (Figure 6a). All animal experiments were performed based on The Care and Use of Laboratory Animals of the Medical Research Council in Xi'an Jiaotong University. The mice were assigned into 6 groups with different treatments: (1) PBS, (2) glucose, (3) glucose + CeO_2, (4) CeO_2/GOx, (5) glucose + GOx, and (6) glucose + CeO_2/GOx. Compared with groups (1−5), the wounds of the mice in group (6) gradually formed scabs and were almost completely healed after 5 days of treatment (Figure 6b). Such phenomenon revealed the serious oxidative damage to the bacterial species induced by ·OH in wounds. The wound areas of the infected sites were determined to compare the therapeutic efficiency. The wound area in group (6) was smaller than the other groups on the 5th day (Figure 6c), suggesting that the ·OH produced by group (6) significantly accelerated the wound-healing process. To evaluate the bactericidal activity, *S. aureus* cells from the wounds of mice were cultured and counted. The bacterial colonies of group (6) decreased obviously compared to groups (1−5) (Figure 6d,e). The antibacterial efficacy of CeO_2/GOx *in vivo* was evaluated to be 99.9%. To assess the effect of wound healing, hematoxylin and eosin staining (H&E) was used for histological analysis. There were many incomplete epidermal layers for groups (1−5), indicating low antibacterial efficiency (Figure 6f). Nevertheless, an intact epidermal structure on the wounds was observed in group (6). The above results demonstrated that the designed CeO_2/GOx nanoreactor exhibited excellent wound-healing performance *in vivo* in the presence of glucose.

3.5. Biosafety of the CeO_2/GOx Nanoreactor. Low toxicity or even nontoxicity of the materials is an important factor for the rational design of antibiotics. The toxicity of the CeO_2/GOx nanoreactor was studied. The CeO_2/GOx nanoreactor exhibited negligible cytotoxicity to HeLa cells (a model cell), with the concentration reaching even 500 μg/mL (Figure S19). For *in vivo* biocompatibility experiments, the CeO_2/GOx nanoreactor was intravenously injected into the mice. The blood biochemical analysis was further performed. The CeO_2/GOx and PBS groups showed similar results (Figure 7a). The body weight was not changed obviously (Figure 7b). Furthermore, there was no obvious inflammation or lesions in the main organs after injection of CeO_2/GOx (Figure 7c). Such results revealed that the CeO_2/GOx nanoreactor showed negligible toxicity.

4. CONCLUSIONS

In summary, a CeO_2/GOx nanoreactor with a mesoporous framework and large internal voids is designed for cascade catalytic antibacterial therapy. The mesoporous CeO_2 hollow spheres are synthesized by thermal decomposition of cerium−polyphenol−formaldehyde polymers. Such mesoporous CeO_2 hollow spheres not only serve as a container to load enzyme molecules but also exhibit peroxidase-like catalytic activity. The mesoporous CeO_2/GOx nanoreactor converts glucose and

https://doi.org/10.1021/acsami.1c10821
ACS Appl. Mater. Interfaces XXXX, XXX, XXX−XXX

oxygen to glucose acid and H_2O_2. The acidic condition would boost the catalytic activity of the mesoporous CeO_2 nanozyme. H_2O_2 molecules are further converted to hydroxyl radicals by the mesoporous CeO_2 nanozyme under the acidic condition. The generated hydroxyl radicals can easily destroy the bacteria cell. Therefore, the CeO_2/GOx nanoreactor exhibits efficient antibacterial performance, which can prevent the formation of biofilms. Moreover, *in vivo* experiments confirm that the nanoreactor possessed superior antibacterial effect and favorable biocompatibility. Compared with the traditional nanozyme antibiotics, such nanoreactors only require nontoxic glucose to generate hydroxyl radicals, which minimize the side effects to healthy tissues. This work provides a general strategy to construct a functional mesoporous nanoreactor for antibacterial therapy, which may be potentially applied in biosensors, therapy, and environmental remediation.

■ ASSOCIATED CONTENT

Supporting Information

The Supporting Information is available free of charge at https://pubs.acs.org/doi/10.1021/acsami.1c10821.

Additional results of characterization studies (SEM, TEM, XRD); synthesis of ceria nanoparticles and cubes; stability assay of CeO_2/GOx cubes; CAT-like activity assay of mesoporous CeO_2 hollow sphere; the relationship between the GOx content and the catalytic property of CeO_2/GOx nanoreactors; live and dead cell fluorescence assay (PDF)

■ AUTHOR INFORMATION

Corresponding Author

Jing Wei − *Institute of Analytical Chemistry and Instrument for Life Science, The Key Laboratory of Biomedical Information Engineering of Ministry of Education, School of Life Science and Technology, Xi'an Jiaotong University, Xi'an, Shaanxi 710049, P. R. China;* orcid.org/0000-0001-9413-2650; Email: jingwei@xjtu.edu.cn

Authors

Jing Qin − *Institute of Analytical Chemistry and Instrument for Life Science, The Key Laboratory of Biomedical Information Engineering of Ministry of Education, School of Life Science and Technology, Xi'an Jiaotong University, Xi'an, Shaanxi 710049, P. R. China*

Youyou Feng − *Institute of Analytical Chemistry and Instrument for Life Science, The Key Laboratory of Biomedical Information Engineering of Ministry of Education, School of Life Science and Technology, Xi'an Jiaotong University, Xi'an, Shaanxi 710049, P. R. China*

Dong Cheng − *Institute of Analytical Chemistry and Instrument for Life Science, The Key Laboratory of Biomedical Information Engineering of Ministry of Education, School of Life Science and Technology, Xi'an Jiaotong University, Xi'an, Shaanxi 710049, P. R. China*

Biwu Liu − *Institute of Analytical Chemistry and Instrument for Life Science, The Key Laboratory of Biomedical Information Engineering of Ministry of Education, School of Life Science and Technology, Xi'an Jiaotong University, Xi'an, Shaanxi 710049, P. R. China;* orcid.org/0000-0001-7357-9875

Zheng Wang − *State Key Laboratory of High-efficiency Utilization of Coal and Green Chemical Engineering, College of Chemistry and Chemical Engineering, Ningxia University, Ningxia 750021, P. R. China;* orcid.org/0000-0002-0265-7546

Yongxi Zhao − *Institute of Analytical Chemistry and Instrument for Life Science, The Key Laboratory of Biomedical Information Engineering of Ministry of Education, School of Life Science and Technology, Xi'an Jiaotong University, Xi'an, Shaanxi 710049, P. R. China;* orcid.org/0000-0002-1796-7651

Complete contact information is available at: https://pubs.acs.org/10.1021/acsami.1c10821

Notes

The authors declare no competing financial interest.

■ ACKNOWLEDGMENTS

This work was financially supported by the National Natural Science Foundation of China (No. 21701130), the Key Research and Development Program of Shaanxi (Program No. 2021GY-225), and the Foundation of State Key Laboratory of High-efficiency Utilization of Coal and Green Chemical Engineering (Grant No. 2020-KF-42). The authors thank Jiao Li and Zijun Ren at the Instrument Analysis Center of Xi'an Jiaotong University for their assistance with TEM analysis.

■ REFERENCES

(1) Hernando-Amado, S.; Coquet, T. M.; Baquero, F.; Martínez, J. L. Defining and Combating Antibiotic Resistance from One Health and Global Health perspectives. *Nat. Microbiol.* **2019**, *4*, 1432−1442.

(2) Cohen, M. L. Epidemiology of Drug Resistance: Implications for a Post-Antimicrobial Era. *Science* **1992**, *257*, 1050−1055.

(3) Sun, H.; Gao, N.; Dong, K.; Ren, J.; Qu, X. Graphene Quantum Dots-Band-Aids Used for Wound Disinfection. *ACS Nano* **2014**, *8*, 6202−6210.

(4) Liu, C.; Kong, D.; Hsu, P. C.; Yuan, H.; Lee, H. W.; Liu, Y.; Wang, H.; Wang, S.; Yan, K.; Lin, D.; Maraccini, P. A.; Parker, K. M.; Boehm, A. B.; Cui, Y. Rapid Water Disinfection Using Vertically Aligned MoS_2 Nanofilms and Visible Light. *Nat. Nanotechnol.* **2016**, *11*, 1098−1104.

(5) Yin, W.; Yu, J.; Lv, F.; Yan, L.; Zheng, L. R.; Gu, Z.; Zhao, Y. Functionalized Nano-MoS_2 with Peroxidase Catalytic and Near-Infrared Photothermal Activities for Safe and Synergetic Wound Antibacterial Applications. *ACS Nano* **2016**, *10*, 11000−11011.

(6) Wang, D.; Zhao, L.; Ma, H.; Zhang, H.; Guo, L. Quantitative Analysis of Reactive Oxygen Species Photogenerated on Metal Oxide Nanoparticles and Their Bacteria Toxicity: the Role of Superoxide Radicals. *Environ. Sci. Technol.* **2017**, *51*, 10137−10145.

(7) Xin, Q.; Shah, H.; Nawaz, A.; Xie, W.; Akram, M.; Batool, A.; Tian, L.; Jan, S.; Boddula, R.; Guo, B.; Liu, Q.; Gong, J. Antibacterial Carbon-Based Nanomaterials. *Adv. Mater.* **2019**, *31*, No. 1804838.

(8) Makvandi, P.; Wang, C.; Zare, E. N.; Borzacchiello, A.; Niu, L.; Tay, F. R. Metal-Based Nanomaterials in Biomedical Applications: Antimicrobial Activity and Cytotoxicity Aspects. *Adv. Funct. Mater.* **2020**, *30*, No. 1910021.

(9) Stankic, S.; Suman, S.; Haque, F.; Vidic, J. Pure and Multimetal Oxide Nanoparticles: Synthesis, Antibacterial and Cytotoxic Properties. *J. Nanobiotechnol.* **2016**, *14*, No. 73.

(10) Huang, Y.; Ren, J.; Qu, X. Nanozymes: Classification, Catalytic Mechanisms, Activity Regulation, and Applications. *Chem. Rev.* **2019**, *119*, 4357−4412.

(11) Liang, M.; Yan, X. Nanozymes: from New Concepts, Mechanisms, and Standards to Applications. *Acc. Chem. Res.* **2019**, *52*, 2190−2200.

(12) Wu, J.; Wang, X.; Wang, Q.; Lou, Z.; Li, S.; Zhu, Y.; Qin, L.; Wei, H. Nanomaterials with Enzyme-Like Characteristics (Nano-

zymes): Next-Generation Artificial Enzymes (II). *Chem. Soc. Rev.* **2019**, *48*, 1004−1076.
(13) Wang, X.; Fan, L.; Cheng, L.; Sun, Y.; Wang, X.; Zhong, X.; Shi, Q.; Gong, F.; Yang, Y.; Ma, Y.; Miao, Z.; Zha, Z. Biodegradable Nickel Disulfide Nanozymes with GSH-Depleting Function for High-Efficiency Photothermal-Catalytic Antibacterial Therapy. *iScience* **2020**, *23*, No. 101281.
(14) Liu, X.; Yan, Z.; Zhang, Y.; Liu, Z.; Sun, Y.; Ren, J.; Qu, X. Two-Dimensional Metal-Organic Framework/Enzyme Hybrid Nanocatalyst as a Benign and Self-Activated Cascade Reagent for *in Vivo* Wound Healing. *ACS Nano* **2019**, *13*, 5222−5230.
(15) Gao, L.; Giglio, K. M.; Nelson, J. L.; Sondermann, H.; Travis, A. J. Ferromagnetic Nanoparticles with Peroxidase-Like Activity Enhance the Cleavage of Biological Macromolecules for Biofilm Elimination. *Nanoscale* **2014**, *6*, 2588−2593.
(16) Dickinson, B. C.; Chang, C. J. Chemistry and Biology of Reactive Oxygen Species in Signaling or Stress Responses. *Nat. Chem. Biol.* **2011**, *7*, 504−511.
(17) Mao, D.; Wan, J.; Wang, J.; Wang, D. Sequential Templating Approach: a Groundbreaking Strategy to Create Hollow Multishelled Structures. *Adv. Mater.* **2019**, *31*, No. 1802874.
(18) Wang, J.; Wan, J.; Wang, D. Hollow Multishelled Structures for Promising Applications: Understanding the Structure-Performance Correlation. *Acc. Chem. Res.* **2019**, *52*, 2169−2178.
(19) Zhu, W.; Chen, Z.; Pan, Y.; Dai, R.; Wu, Y.; Zhuang, Z.; Wang, D.; Peng, Q.; Chen, C.; Li, Y. Functionalization of Hollow Nanomaterials for Catalytic Applications: Nanoreactor Construction. *Adv. Mater.* **2019**, *31*, No. 1800426.
(20) Wang, J.; Wan, J.; Yang, N.; Li, Q.; Wang, D. Hollow Multishell Structures Exercise Temporal-Spatial Ordering and Dynamic Smart Behaviour. *Nat. Rev. Chem.* **2020**, *4*, 159−168.
(21) Wang, J.; Cui, Y.; Wang, D. Design of Hollow Nanostructures for Energy Storage, Conversion and Production. *Adv. Mater.* **2019**, *31*, No. 1801993.
(22) Jeong, S. Y.; Kim, J. S.; Lee, J. H. Rational Design of Semiconductor-Based Chemiresistors and Their Libraries for Next-Generation Artificial Olfaction. *Adv. Mater.* **2020**, *32*, No. 2002075.
(23) Dang, S.; Zhu, Q. L.; Xu, Q. Nanomaterials Derived from Metal-Organic Frameworks. *Nat. Rev. Mater.* **2018**, *3*, No. 17075.
(24) Wang, G.; Qin, J.; Feng, Y.; Feng, B.; Yang, S.; Wang, Z.; Zhao, Y.; Wei, J. Sol-Gel Synthesis of Spherical Mesoporous High-Entropy Oxides. *ACS Appl. Mater. Interfaces* **2020**, *12*, 45155−45164.
(25) Wang, G.; Qin, J.; Zhou, X.; Deng, Y.; Wang, H.; Zhao, Y.; Wei, J. Self-Template Synthesis of Mesoporous Metal Oxide Spheres with Metal-Mediated Inner Architectures and Superior Sensing Performance. *Adv. Funct. Mater.* **2018**, *28*, No. 1806144.
(26) Liu, B.; Sun, Z.; Huang, P. J. J.; Liu, J. Hydrogen Peroxide Displacing DNA from Nanoceria: Mechanism and Detection of Glucose in Serum. *J. Am. Chem. Soc.* **2015**, *137*, 1290−1295.
(27) Montini, T.; Melchionna, M.; Monai, M.; Fornasiero, P. Fundamentals and Catalytic Applications of CeO_2-Based Materials. *Chem. Rev.* **2016**, *116*, 5987−6041.
(28) Singh, S. Cerium Oxide Based Nanozymes: Redox Phenomenon at Biointerfaces. *Biointerphases* **2016**, *11*, No. 04B202.
(29) Heckert, E. G.; Karakoti, A. S.; Seal, S.; Self, W. T. The Role of Cerium Redox State in the SOD Mimetic Activity of Nanoceria. *Biomaterials* **2008**, *29*, 2705−2709.
(30) Xia, T.; Kovochich, M.; Liong, M.; Maedler, L.; Gilbert, B.; Shi, H.; Yeh, J. I.; Zink, J. I.; Nel, A. E. Comparison of the Mechanism of Toxicity of Zinc Oxide and Cerium Oxide Nanoparticles Based on Dissolution and Oxidative Stress Properties. *ACS Nano* **2008**, *2*, 2121−2134.
(31) Xu, C.; Qu, X. Cerium Oxide Nanoparticle: a Remarkably Versatile Rare Earth Nanomaterial for Biological Applications. *NPG Asia Mater.* **2014**, *6*, No. e90.
(32) Tian, Z.; Li, J.; Zhang, Z.; Gao, W.; Zhou, X.; Qu, Y. Highly Sensitive and Robust Peroxidase-Like Activity of Porous Nanorods of Ceria and Their Application for Breast Cancer Detection. *Biomaterials* **2015**, *59*, 116−124.
(33) Herget, K.; Hubach, P.; Pusch, S.; Deglmann, P.; Goetz, H.; Gorelik, T. E.; Gural'skiy, I.; Pfitzner, F.; Link, T.; Schenk, S.; Panthoefer, M.; Ksenofontov, V.; Kolb, U.; Opatz, T.; Andre, R.; Tremel, W. Haloperoxidase Mimicry by CeO_2-x Nanorods Combats Biofouling. *Adv. Mater.* **2017**, *29*, No. 1603823.
(34) Wang, Z.; Yu, R. Hollow Micro/Nanostructured Ceria-Based Materials: Synthetic Strategies and Versatile Applications. *Adv. Mater.* **2019**, *31*, No. 1800592.
(35) Huo, M.; Wang, L.; Chen, Y.; Shi, J. Tumor-Selective Catalytic Nanomedicine by Nanocatalyst Delivery. *Nat. Commun.* **2017**, *8*, No. 357.
(36) Yang, Y.; Lu, Y.; Abbaraju, P.; Azimi, I.; Lei, C.; Tang, J.; Jambhrunkar, M.; Fu, J.; Zhang, M.; Liu, Y.; Liu, C.; Yu, C. Stepwise Degradable Nanocarriers Enabled Cascade Delivery for Synergistic Cancer Therapy. *Adv. Funct. Mater.* **2018**, *28*, No. 1800706.
(37) Fan, W.; Lu, N.; Huang, P.; Liu, Y.; Yang, Z.; Wang, S.; Yu, G.; Liu, Y.; Hu, J.; He, Q.; Qu, J.; Wang, T.; Chen, X. Glucose-Responsive Sequential Generation of Hydrogen Peroxide and Nitric Oxide for Synergistic Cancer Starving-Like/Gas Therapy. *Angew. Chem., Int. Ed.* **2017**, *56*, 1229.
(38) Yu, Z.; Zhou, P.; Pan, W.; Li, N.; Tang, B. A Biomimetic Nanoreactor for Synergistic Chemiexcited Photodynamic Therapy and Starvation Therapy Against Tumor Metastasis. *Nat. Commun.* **2018**, *9*, No. 5044.
(39) Li, J.; Li, Y.; Wang, Y.; Ke, W.; Chen, W.; Wang, W.; Ge, Z. Polymer Prodrug-Based Nanoreactors Activated by Tumor Acidity for Orchestrated Oxidation/Chemotherapy. *Nano Lett.* **2017**, *17*, 6983.
(40) Li, J.; Dirisala, A.; Ge, Z.; Wang, H.; Yin, W.; Ke, W.; Toh, K.; Xie, J.; Matsumoto, Y.; Anraku, Y.; Osada, K.; Kataoka, K. Therapeutic Vesicular Nanoreactors with Tumor-Specific Activation and Self-Destruction for Synergistic Tumor Ablation. *Angew. Chem., Int. Ed.* **2017**, *56*, 14025.
(41) Zhao, W.; Hu, J.; Gao, W. Glucose Oxidase-Polymer Nanogels for Synergistic Cancer-Starving and Oxidation Therapy. *ACS Appl. Mater. Interfaces* **2017**, *9*, 23528.
(42) Zhang, L.; Wan, S.; Li, C.; Xu, L.; Cheng, H.; Zhang, X. An Adenosine Triphosphate-Responsive Autocatalytic Fenton Nanoparticle for Tumor Ablation with Self-Supplied H2O2 and Acceleration of Fe(III)/Fe(II) Conversion. *Nano Lett.* **2018**, *18*, 7609.
(43) Cheng, H.; Jiang, X.; Zheng, R.; Zuo, S.; Zhao, L.; Fan, G.; Xie, B.; Yu, X.; Li, S.; Zhang, X. A Biomimetic Cascade Nanoreactor for Tumor Targeted Starvation Therapy-Amplified Chemotherapy. *Biomaterials* **2019**, *195*, 75.
(44) Chen, W.; Vázquez-González, M.; Zoabi, A.; Abu-Reziq, R.; Willner, I. Biocatalytic Cascades Driven by Enzymes Encapsulated in Metal-Organic Framework Nanoparticles. *Nat. Catal.* **2018**, *1*, 689.
(45) Chen, G.; Huang, S.; Kou, X.; Wei, S.; Huang, S.; Jiang, S.; Shen, J.; Zhu, F.; Ouyang, G. A Convenient and Versatile Amino-Acid-Boosted Biomimetic Strategy for the Nondestructive Encapsulation of Biomacromolecules within Metal-Organic Frameworks. *Angew. Chem., Int. Ed.* **2019**, *58*, 1463.
(46) Liu, Z.; Li, T.; Han, F.; Wang, Y.; Gan, Y.; Shi, J.; Wang, T.; Akhtarc, M.; Li, Y. A Cascade-Reaction Enabled Synergistic Cancer Starvation/ROS-Mediated/Chemo-Therapy with an Enzyme Modified Fe-Based MOF. *Biomater. Sci.* **2019**, *7*, 3683.
(47) Feng, L.; Xie, R.; Wang, C.; Gai, S.; He, F.; Yang, D.; Yang, P.; Lin, J. Magnetic Targeting, Tumor Microenvironment-Responsive Intelligent Nanocatalysts for Enhanced Tumor Ablation. *ACS Nano* **2018**, *12*, 11000.
(48) Wei, J.; Wang, G.; Chen, F.; Bai, M.; Liang, Y.; Wang, H.; Zhao, D.; Zhao, Y. Sol-Gel Synthesis of Metal-Phenolic Coordination Spheres and Their Derived Carbon Composites. *Angew. Chem., Int. Ed.* **2018**, *57*, 9838−9843.
(49) Feng, B.; Feng, Y.; Qin, J.; Wang, Z.; Zhang, Y.; Du, F.; Zhao, Y.; Wei, J. Self-Template Synthesis of Spherical Mesoporous Tin Dioxide from Tin-Polyphenol-Formaldehyde Polymers for Conductometric Ethanol Gas Sensing. *Sens. Actuators, B* **2021**, *341*, No. 129965.

https://doi.org/10.1021/acsami.1c10821
ACS Appl. Mater. Interfaces XXXX, XXX, XXX−XXX

(50) Yang, Y.; Mao, Z.; Huang, W.; Liu, L.; Li, J.; Li, J.; Wu, Q. Redox Enzyme-Mimicking Activities of CeO_2 Nanostructures: Intrinsic Influence of Exposed Facets. *Sci. Rep.* **2016**, *6*, No. 35344.
(51) Bêche, E.; Charvin, P.; Perarnau, D.; Abanades, S.; Flamant, G. Ce 3d XPS Investigation of Cerium Oxides and Mixed Cerium Oxide ($Ce_xTi_yO_z$). *Surf. Interface Anal.* **2008**, *40*, 264−267.
(52) Li, M. M.; Wang, P. F.; Ji, Z. Z.; Zhou, Z. R.; Xia, Y. G.; Li, Y.; Zhan, S. H. Efficient Photocatalytic Oxygen Activation by Oxygen-Vacancy-Rich CeO_2-Based Heterojunctions: Synergistic Effect of Photoexcited Electrons Transfer and Oxygen Chemisorption. *Appl. Catal., B* **2021**, *289*, No. 120020.
(53) Celardo, I.; De Nicola, M.; Mandoli, C.; Pedersen, J.; Ghibelli, L. Ce^{3+} Ions Determine Redox-Dependent Anti-Apoptotic Effect of Cerium Oxide Nanoparticles. *ACS Nano* **2011**, *6*, 4537−4549.
(54) Pirmohamed, T.; Dowding, J.; Singh, S.; Wasserman, B.; Heckert, E.; Karakoti, A.; King, J.; Seal, S.; Self, W. Nanoceria Exhibit Redox State-Dependent Catalase Mimetic Activity. *Chem. Commun.* **2010**, *46*, 2736−2738.
(55) Skorodumova, N.; Simak, S.; Lundqvist, B.; Abrikosov, I.; Johansson, B. Quantum Origin of the Oxygen Storage Capability of Ceria. *Phys. Rev. Lett.* **2002**, *89*, No. 166601.
(56) Heckert, E.; Seal, S.; Self, W. Fenton-Like Reaction Catalyzed by the Rare Earth Inner Transition Metal Cerium. *Environ. Sci. Technol.* **2008**, *42*, 5014−5019.
(57) Asati, A.; Santra, S.; Kaittanis, C.; Nath, C. S.; Perez, J. Oxidase-Like Activity of Polymer-Coated Cerium Oxide Nanoparticles. *Angew. Chem., Int. Ed.* **2009**, *48*, 2308−2312.
(58) Tan, F.; Zhang, Y.; Wang, J.; Wei, J.; Cai, Y.; Qian, X. An Efficient Method for Dephosphorylation of Phosphopeptides by Cerium Oxide. *J. Mass Spectrom.* **2008**, *43*, 628−632.
(59) Chen, G.; Huang, S.; Kou, X.; Wei, S.; Huang, S.; Jiang, S.; Shen, J.; Zhu, F.; Ouyang, G. A Convenient and Versatile Amino-Acid-Boosted Biomimetic Strategy for the Nondestructive Encapsulation of Biomacromolecules within Metal-Organic Framework. *Angew. Chem., Int. Ed.* **2019**, *58*, 1463−1467.
(60) Liu, Y.; Lin, A.; Liu, J.; Chen, X.; Zhu, X.; Gong, Y.; Yuan, G.; Chen, L.; Liu, J. Enzyme-Responsive Mesoporous Ruthenium for Combined ChemoPhotothermal Therapy of Drug-Resistant Bacteria. *ACS Appl. Mater. Interfaces* **2019**, *11*, 26590−26606.
(61) Dwyer, D. J.; Kohanski, M. A.; Collins, J. J. Role of Reactive Oxygen Species in Antibiotic Action and Resistance. *Curr. Opin. Microbiol.* **2009**, *12*, 482−489.
(62) Yan, Z.; Bing, W.; Ding, C.; Dong, K.; Ren, J.; Qu, X. A H_2O_2-Free Depot for Treating Bacterial Infection: Localized Cascade Reactions to Eradicate Biofilms: *In Vivo*. *Nanoscale* **2018**, *10*, 17656−17662.
(63) Vatansever, F.; de Melo, W. C. M. A.; Avci, P.; Vecchio, D.; Sadasivam, M.; Gupta, A.; Chandran, R.; Karimi, M.; Parizotto, N. A.; Yin, R.; Tegos, G. P.; Hamblin, M. R. Antimicrobial Strategies Centered Around Reactive Oxygen Species-Bactericidal Antibiotics, Photodynamic Therapy, and Beyond. *FEMS Microbiol. Rev.* **2013**, *37*, 955−989.
(64) Liang, M.; Wang, Y.; Ma, K.; Yu, S.; Chen, Y.; Deng, Z.; Liu, Y.; Wang, F. Engineering Inorganic Nanoflares with Elaborate Enzymatic Specificity and Efficiency for Versatile Biofilm Eradication. *Small* **2020**, *16*, No. 2002348.

https://doi.org/10.1021/acsami.1c10821
ACS Appl. Mater. Interfaces XXXX, XXX, XXX−XXX